

Received May 23, 2021; reviewed; accepted October 23, 2021

The removal of Fe from the reduced ilmenite via aeration leaching - assessing the effect of operating parameters

Siti Asmidar Ibrahim ¹, Farhana Yunus ¹, Kamar Shah Ariffin ¹, Sheikh Abdul Rezan Sheikh Abdul Hamid ¹, Suhaina Ismail ¹, Nurul Ain Jabit ¹

¹ Mineral Strategy Niche Group, School of Material and Mineral Resources Engineering, Universiti Sains Malaysia, 14300 Nibong Tebal, Penang, Malaysia

Corresponding author: ainjabit@usm.my (Nurul Ain Jabit)

Abstract: An upgrade of Malaysian ilmenite (FeTiO_3) concentrate to synthetic rutile (TiO_2) using aeration leaching was investigated in this study. Carbothermal reduction using Sarawak Mukah-Balingan coal and compressed National Gas (CNG) as a reductant was used to produce reduced ilmenite (RI) as an intermediate phase consisting of titanium oxide matrix with metallic iron prior to aeration leaching. Metallic iron was dissolved in ammonium chloride solution after the reduction process, separating synthetic rutile in the leaching residue. This study aims to evaluate the leaching parameters, such as concentration, temperature, and leaching time. The optimum conditions established by the design of the experiment (DOE) and the analysis of variance (ANOVA) has indicated that leaching temperature was the most significant parameter for iron dissolution. It was found that iron dissolution at a maximum value of 97.0% was achieved at an optimum condition of 0.5 M NH_4Cl at 90°C for 7 hours. With an initial weight of 46 wt.% TiO_2 and 37 wt.% Fe_2O_3 , ilmenite was successfully upgraded to 80 wt.% and 8 wt.%, respectively. In conclusion, Malaysian ilmenite has a high potential value to be upgraded to synthetic rutile by aeration leaching with ammonium chloride via Becher process.

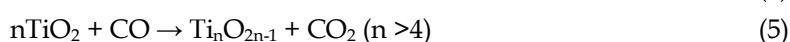
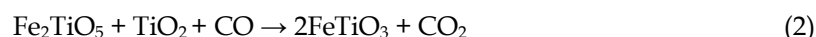
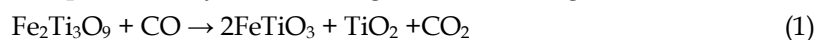
Keywords: ilmenite, reduced ilmenite, aeration leaching, synthetic rutile, titanium dioxide

1. Introduction

Titanium dioxide (TiO_2) is the most common titanium product, primarily in energy and environmental applications such as catalysis, photocatalysis, antibacterial agents, and civil applications such as nano paint (self-cleaning). It is also popular as a filler in the paper, plastic and rubber industries (Gázquez et al., 2014; Haider et al., 2020). Titanium can be found naturally in several types of rocks and minerals sands, for instance, rutile (98.5-97.0 wt.% TiO_2), ilmenite (38.5-61.0 wt.% TiO_2), anatase, leucosene, including other titanium minerals. Owing to the inability of developing natural rutile resources, ilmenite has been upgraded to synthetic rutile (SR) (>90 wt.% TiO_2) as a feedstock for titanium dioxide and titanium metal production industries (Zhang et al., 2011; Rezan et al., 2012). Ilmenite is known as iron(II) titanium with a chemical formula of FeTiO_3 . The crystal structure of ilmenite is hexagonal that consists of alternating layers of Ti^{4+} and Fe^{2+} ions. Naturally, the titanium dioxide composition in ilmenite was about 47 wt.% (Heiken et al., 1991).

There have been various processes to manufacture synthetic rutile from ilmenite ores, such as Becher process, Benelite process, Austpac process, and Murso Process (Filippou and Hudon, 2009; Zhang et al., 2011; Shahien et al., 2015; Wang et al., 2018; Nguyen and Lee, 2019;). Benelite process implements carbon thermo-reduction reaction for alternating ferric iron to ferrous state and subsequently eliminated through hydrochloric acid leaching. In the Austpac process, magnetite ilmenite is formed after being roasted to withdraw any gangue minerals through magnetic separation and the hydrochloric acid leaching process. Meanwhile, for the Murso process, oxidation and reduction of ilmenite occur, and

hydrochloric acid leaching is utilised to separate titanium and waste substances. For the Becher process, both pyrometallurgical and hydrometallurgical routes take place by performing two crucial steps: reduction and aeration (Ahmadi et al., 2017; Ahmadi et al., 2018; Xiang et al., 2020). Ilmenite contains impurities such as iron, which result in its low grade and is difficult to separate directly by physical separation. Thus, iron is converted to soluble ferrous or elemental forms by reducing the high temperature, followed by acid leaching to obtain a synthetic rutile product. The ferrous and ferric content of the ilmenite was first reduced to metallic iron in a rotary kiln at ~1500 °C using coal as fuel and reductant. These changes can be represented by the following reactions (Xiang et al., 2020):



The metallic iron is then removed from reduced ilmenite by aeration leaching using 1% ammonium chloride with air/oxygen at elevated temperatures. The leaching process will form a mixture of fine (0.1-0.1 μm) iron oxides (Fe₂O₃, Fe₃O₄) and oxyhydroxides (alpha or gamma Fe₂O₃.xH₂O) and coarse titanium dioxide particles. The following half-cell reactions can represent the removal of metallic iron:



The oxidation of ferrous ions is then given by:



The commercial Becher process offers a few advantages on environment and cost. It produces almost neutral leachate, low consumption of reagents, and the by-product "red mud" can be utilised as raw material for the iron making process. It also operates at low capital and operating cost. However, this process also has few drawbacks which is quite a significant factor that affects its efficiency. The aeration leaching is extremely sluggish, which takes more than 22 hours to dissolve the iron (Xiang et al., 2020). Leaching time and iron removal rate have been reported elsewhere to be accelerated by using catalysts such as acetic, tartaric, citric acid or anthraquinone derivatives (Warren et al., 2004; Truong et al., 2017), etc. This catalyst can be differentiated based on efficiency, electrochemical activity and cost.

This work aims to study the potential of Malaysian ilmenite ore to be upgraded to synthetic rutile by adapting Becher process techniques. The second objective of this study was to determine the significant parameters of aeration leaching on reduced ilmenite using statistical approaches.

2. Experimental work

2.1. Materials

The raw materials used in this study was low-grade ilmenite ores from Sungai Cheniah, Bukit Kelip, Dungun Terengganu in the East of Malaysia (Yaakub et al., 2016). About 4.0 kg of ilmenite samples were obtained using a panning method from the riverbank, and it was further concentrated by using magnetic separation. The chemical composition before and after the concentration process is presented in Table 1. All the other reagents used for leaching and chemical analysis were analytical grade and purity greater than 99.9%.

Table 1. Chemical composition of ilmenite ore and ilmenite concentrate (wt.%)

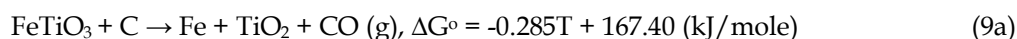
Sample	TiO ₂	Fe ₂ O ₃	SiO ₂	MnO	Al ₂ O ₃	MgO	CaO	RuO ₂	ZrO ₂	K ₂ O	NbO
Ilmenite ore	46.71	37.10	8.39	2.92	2.02	1.65	0.64	0.25	0.18	0.06	0.04
Ilmenite concentrate*	47.26	39.87	5.13	2.06	1.82	1.62	0.57	-	-	-	-

* Ilmenite sample after screening and magnetic separation process

2.2. Experimental procedure

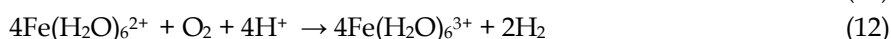
2.2.1. Carbothermal reduction

Carbothermal reduction was conducted at specific temperatures using Sarawak Mukah-Balingan coal as local carbon source and CNG as the reducing agent or reductant. For this research, an isothermal reduction approach was used. This isothermal reaction was conducted at high temperature to ensure the wanted oxides reacted and being reduced. The carbothermal reduction was carried out in a 90% Ar-10% CNG gas mixture for 3 hours at 1250 °C. The flow rate was set to 1.5 dm³/min and argon gas was allowed to flow until the temperature has decreased to room temperature. Further details of the experimental setup was published elsewhere (Yin et al., 2017). The gas mixture of argon and CNG was aimed to reduce excessive carbon deposition while the use of Sarawak Mukah-Balingan coal in carbothermal reduction was adapted from Ibrahim et al. (2017) that have successfully converted ilmenite to nitrated ilmenite. The carbon to reducible oxygen molar ratio was set at 1:1.5. The experiments were conducted in a horizontal Lenton tube electric furnace with molybdenum disilicide heating elements. After completion, the reduced samples were cooled down to room temperature in the same gas flow to avoid re-oxidation. For the isothermal reduction experiments, the heating rate and cooling rate were set to 10 °C per minute while soaking time at 1250 °C was 180 minutes. The overall equation for the carbothermal reduction process is shown in Eq. 9a and 9b. Both reactions are favourable above 1200 °C.



2.2.2. Aeration leaching

A three-necked round-bottom reaction flask of 250 cm³ capacity was used in the aeration leaching study. A magnetic bar was used as an agitator for the solution in the reaction vessel. A temperature-controlled magnetic hot plate was used to regulate the solution's temperature inside the reaction vessel and a silicone oil bath to control the temperature of the solution. The air (2.5 dm³/min) was supplied through the solution using a plastic tube connected to a diaphragm pump. The solution was heated until it reached the desired temperature, and 4.0 g of reduced ilmenite with particle size fraction of -75-50 μm was added to the reaction vessel. The oxidation of ferrous iron in the leaching process can be described by the following reactions (Geetha and Surender, 2000).



The temperature of the solution was monitored regularly to ensure the operating temperature remained constant. After the experiment was completed, the solution was filtered using 45 μm Whatman filter paper. The filtrate was washed with distilled water and dilute HCl solutions to remove any traces of iron. The filtered cake was dried in the furnace at 100 °C for 24 hours and subsequently ground into fine powder. This fine powder will be subjected to characterisation analysis. All filtered solution was analysed by Inductively Coupled Plasma-Optical Emission Spectroscopy (ICP-OES) (Perkin Elmer Optima 4300 DV ICP System) to determine the concentration of iron (Fe), within the analysed solution.

2.2.3. Experimental design by full factorial design (FFD)

In this section, the investigated factors (i.e. parameters) were NH₄Cl molarity concentration (A), leaching time (B) in hours (h) and leaching temperature (C) in degree centigrade (°C). The stirring rate (300rpm) and solid to liquid ratio (1:40) were kept constant in this experiment. In this experimental setup, the leaching process was performed using 2³ + s where s is the central point. The central point was set to 3, similar to work done by Francis and El-Midany (2008). This factorial design elucidates the main effect and interaction effect of the investigated factor. The parameters and corresponding levels investigated are presented in Table 2. MiniTab 18 software was used for the analysis of the result.

2.2. Characterisation of reduced ilmenite and leaching residue

The products obtained after carbothermal reduction and aeration leaching were required to undergo

Table 2. Parameters and corresponding level tested in the leaching studies

Parameter	Coding	Unit	Levels		
			-1	0	1
NH ₄ Cl Concentration	A	M	0.1	0.3	0.5
Time	B	h	3	5	7
Temperature	C	°C	50	70	90

Table 3. Experimental runs of 2³ +s factorial design for aeration leaching

Run No	Natural Variables			Coded Factor		
	NH ₄ Cl Concentration	Time	Temperature	A	B	C
1	0.5	7	50	+	+	-
2	0.5	3	90	+	-	+
3	0.5	3	50	+	-	-
4	0.1	7	90	-	+	+
5	0.1	3	50	-	-	-
6	0.5	7	90	+	+	+
7	0.3	5	70	0	0	0
8	0.3	5	70	0	0	0
9	0.3	5	70	0	0	0
10	0.1	7	50	-	+	-
11	0.1	5	90	-	-	+

careful characterisation analysis. This was to understand their composition, phase and morphology, before and after the experiment. The identification of phases on representative samples was performed using XRD analysis method with Cu-K α radiation (Bruker D8 Advanced XRD. All minerals were identified with PANalytical X'Pert HighScore Plus software (v2.2e) and the PANalytical ICSD database. The morphological of the samples were studied using field emission scanning electron microscopy with energy dispersive X-ray analysis (FESEM/EDX; Gemini SUPRA 35VP-ZEISS). First, the samples must be sputter with gold to cover the specimen with a layer of conducting material. Then, the samples were observed under the SEM and images were taken at a different working distance and accelerating voltage to produce Backscattered Electrons Images (BSE) for each sample.

3. Results and discussion

3.1. Characterisation of reduced ilmenite

Before the aeration leaching can proceed, it is vital to evaluate the quality of the reduced ilmenite by confirming that all iron oxides have been converted to metallic iron. The backscattered photomicrograph of the raw ilmenite sample and reduced ilmenite sample after carbothermal reduction (CR) are shown in Fig. 1. Fig.1a indicates the different morphologies of the ilmenite sample before carbothermal reduction. The main components identified (via EDX) are iron (30%) and titanium (38%), possibly ilmenite with shades of grey (as marked in the blue box). In the few altered grains, micro-veinlet of quartz cross-cut the ilmenite grains (dark grey) was observed as marked in the red box. Similar findings were also observed by Yaraghi et al. (2016). Fig. 1b and c display the morphology of reduced ilmenite carried out at 1250 °C for 3 hours in Argon-CNG gas mixture. It can be seen that after carbothermal reduction, the metallic iron or iron carbide appears resulted from the conversion of Fe²⁺ to Fe (white shade colour that pointed by red arrows). At high magnification (Fig. 1d), the spot analyses using EDX showing the elemental composition at different grey shades levels (Table 4). At spot 1, EDX analyses indicated that the metallic phase formed was mainly iron (81.5 wt.%) with little presence of carbon (18.5 wt.%). In the region of dark grey shades (spot 2) showed a high content of Si with little presence of Ti and Fe. At spot 3, EDX analysis indicated that the greyish shade consists of Fe (81.6 wt %), Ti (1.3 wt %) and C with 16.4 wt %. While in the area of grey shades (Spot 4) consist of Fe (21.6 wt.%),

Ti (24.0 wt.%) and O (54.4 wt.%). The results from SEM and EDX analyses showed that the formation of metallic iron during CR was successful. However, it can be seen that in some areas, iron oxides were not converted to metallic iron as shown in Fig. 1d. This is due to Si inclusion in Fe and Ti matrix, which hindered the reduction of Fe^{2+} to Fe metal.

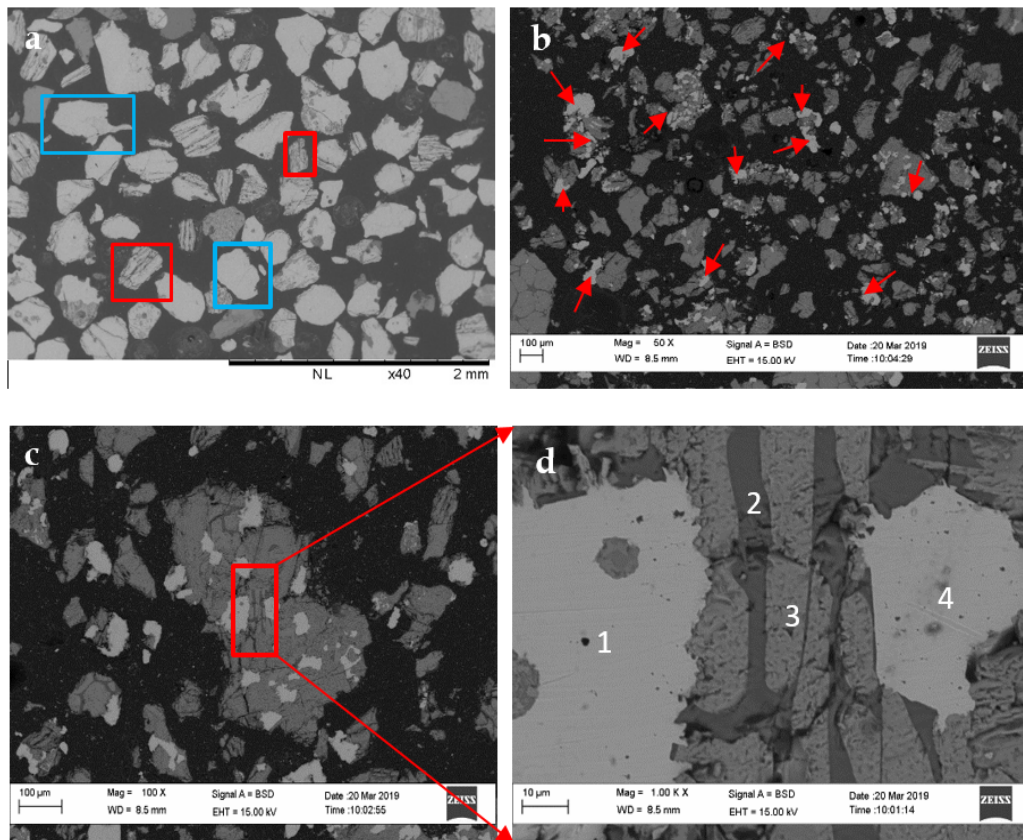


Fig. 1. Backscattered electron photomicrograph of the (a) raw ilmenite ore, (b) reduced ilmenite at carbon to oxygen molar ratio 1:1.4, (c) reduced ilmenite grains and (d) reduced ilmenite

Table 4. Selected EDX spot analyses of the reduced ilmenite grain as seen in Fig. 1d

Analysed Spot	Composition (wt.%)					
	Fe	Ti	C	Si	Nb	O
1	81.5	-	18.5	-	-	-
2	9.1	3.3	35.3	52.3	-	-
3	81.6	1.3	16.4	-	0.7	-
4	21.6	24.0	-	-	-	54.4

The XRD pattern of reduced and raw ilmenite is illustrated in Fig. 2. From XRD analysis, only the ilmenite (FeTiO_3), ICSD# 98-001-7093 phase can be identified in the raw ilmenite samples. After carbothermal reduction, only iron peaks (ICSD No: 98-002-2045), TiC (ICSD No: 98-008-5911), and Ti_2O_3 (ICSD No: 01-085-0868) was identified. This indicated that the reduction of iron oxide in ilmenite to metallic iron (Fe) had occurred accordingly, as shown in Eq. 9a and 9b. In ilmenite reduction by solid carbon or methane in CNG, iron oxides were reduced to metallic iron. Titanium oxides can be reduced to titanium carbide (oxycarbide), which strongly depends on the reduction temperature (Adipuri et al., 2011).

3.2. Thermodynamic studies on the ilmenite sample

Thermodynamic modelling was undertaken to understand the phase stability at the carbothermal reduction temperature. To predict the occurrence of a reaction at a specific temperature and gas atmos-

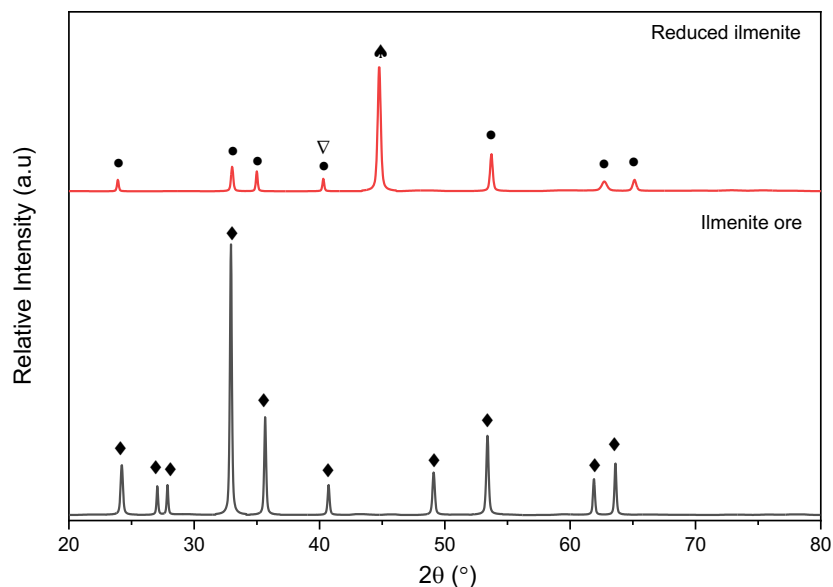


Fig. 2. The XRD diffractogram pattern of the unreduced ilmenite (raw ilmenite ore) and the reduced ilmenite. (♦ FeTiO₃; ●: Ti₂O₃; ▲: Fe; ▽: TiC)

phere by displaying the chemical phases formed during reduction and leaching, HSC Chemistry software v6.0 was used for the thermodynamic modelling aspect of this work. The thermo analysis of the carbothermal reduction of ilmenite is given in Table 5, showing the values of the standard Gibbs free energy, ΔG , and the temperature (T) at equilibrium for each reaction. TiC and Ti(O,C) formation can only be produced above 1573 K when Argon gas with excess carbon content was used (Dewan et al., 2009; Dewan et al., 2010). Firstly, the ilmenite was reduced to iron and TiO₂ phases.

During the reduction of TiO₂ to magneli phases, it was also converted into several phases, including Ti₃O₅. The reduction of ilmenite concentrates in an inert atmosphere was incomplete after 300 minutes at 1573 K unless CNG was added as an excess carbon to enhance reduction. CNG will break down to H₂ and C above 973 K. The introduction of H₂ will enhance the reduction of TiO₂ to magneli phases and later into TiC and Ti(O,C). Without H₂ and N₂, Ti(O,C) formation via Ti₃O₅ pathway was not observed (Sharifah et al., 2013). The ilmenite phase was not fully converted to TiO₂ and resulted in the production of Ti₂O₃. This was proven by Dewan et al. (2010) and Hasniyati et al. (2014). Therefore, to achieve high purity TiO₂, excess carbons and H₂ gas must be added to the ilmenite reduction by increasing the carbon to reducible oxygen molar ratio via CNG. Furthermore, CNG or LPG was chosen due to its abundance in Malaysia compared to coal.

Table 5. Ilmenite and titanium reactions, Gibbs free energy (ΔG°) and temperature (T)

Reaction	ΔG° (kJ/mole)	T _{eq} (K)
FeTiO ₃ + C = Fe + TiO ₂ + CO(g)	200.44-0.35T	573.83
Fe ₂ O ₃ + 3C = 2Fe + 3CO(g)	489.35-0.51T	954.83
3TiO ₂ + C = Ti ₃ O ₅ + CO(g)	283.20-0.2T	1401.98
2Ti ₃ O ₅ + C = 3Ti ₂ O ₃ + CO(g)	241.31-0.14T	1704.16
Ti ₂ O ₃ + C = 2TiO + CO(g)	322.63-0.17T	1918.13
TiO ₂ + 3C = TiC + 2CO(g)	536.62-0.335T	1601.37
CH ₄ (g) + Fe = C + 2H ₂ (g) + Fe	58.589-0.10T	544.51

The standard Gibbs free energy was plotted against temperature from 273.15 to 1773.15 K (Fig. 3a). The values of ΔG° (kJ/mole) for the formation of Ti₃O₅, TiO₂, TiC, Ti₂O₃ and Fe were found to be negative over the temperature range investigated due to favourable reactions. It also depicts that iron formation was the most favourable and started to form at 900 K whilst Ti₂O₃ required a higher

temperature to initiate the reaction (more than 1000 K) before obtaining the TiO_2 . The predominance diagram of Ti-O-C system is shown in Fig. 3b. However, there was a limitation in this modelling module where it can only support three elements, and this was not suitable for complex systems involving many elements. At higher partial pressure of gaseous carbon, TiO_2 can be transformed directly to TiC at elevated temperature (850 – 900°C), without going through the formation of suboxides. Theoretically, the TiO_2 will undergo rapid phase transformation to Ti_5O_9 . However, in the actual experimental condition, this phase was not detected due to the presence of excess carbon, CO and H_2 , which rapidly reduced Ti_5O_9 into Ti_3O_5 and subsequently into Ti_2O_3 . Experimental work by Saidin et al. (2014) also demonstrated that this transformation occurred via this pathway. In the reactor, the partial pressure of oxygen depends on many factors, such as the purification of gases used and the concentration of CO formed. Thus, at elevated temperature (more than 1200 °C) at a high partial pressure of CO, TiC or Ti(O,C) can be formed. The pourbaix diagram for Becher process is shown in Fig. 3c below. Experimental evidence for successful Becher process at the conditions listed by the author was presented elsewhere (Ahmadi et al., 2018). Besides this, the thermodynamics and kinetics of the leaching process have been explained elsewhere for the sulfuric acid system which applies to the Becher process (Sanjith et al., 2019). Any sub-oxides phases such as Ti_3O_5 , Ti_2O and Ti(OC) formed in the RI can be easily oxidised back to TiO_2 during the Becher process or subsequent calcination.

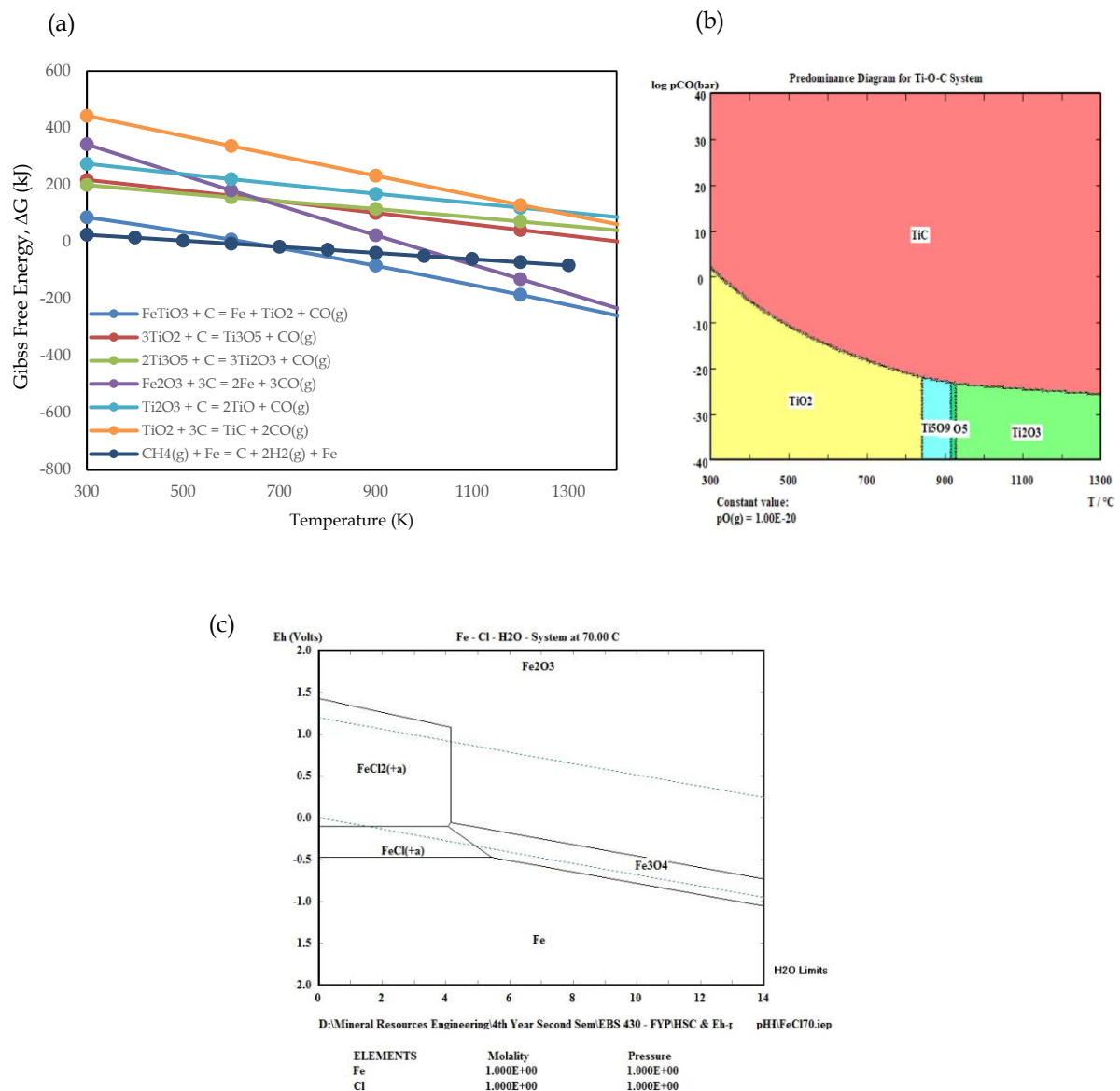


Fig. 3. (a) The plot of ΔG° versus Temperature (K); (b) The predominance diagram for Ti-O-C system at 1300°C; (c) The Pourbaix-diagram for the Fe-Cl-H₂O system

3.3. Statistical analysis of response

In this study, the first set of statistical analysis was performed to investigate the influence of NH_4Cl concentration (A), leaching time (B) and temperature (C) in Fe extraction (%), as well as to estimate the statistical errors by factorial design. The higher level of variables was designated as '+', and the lower level was designated as '-'. The central point was run at medium level and was designated as '0'. Statistical analysis was performed to analyse the effects of each parameter and the interactions between them on the response by using a factorial model. Table 6 shows the results of factorial design ($2^3 + s$) in terms of Fe extraction. The table shows that the highest Fe extraction (97.08 %) was achieved when all variables were set to their maximum value.

Table 6. Result of $2^3 + s$ factorial design: process data for fitting the first-order model

Run No	Natural Variables			Coded Factor			Fe Extraction* (%)
	NH_4Cl Concentration	Time	Temperature	A	B	C	
1	0.5	7	50	+	+	-	63.49
2	0.5	3	90	+	-	+	92.55
3	0.5	3	50	+	-	-	45.86
4	0.1	7	90	-	+	+	83.20
5	0.1	3	50	-	-	-	3.54
6	0.5	7	90	+	+	+	97.08
7	0.3	5	70	0	0	0	59.08
8	0.3	5	70	0	0	0	48.91
9	0.3	5	70	0	0	0	42.94
10	0.1	7	50	-	+	-	40.40
11	0.1	3	90	-	-	+	51.68

*% Fe Extraction = $100 \times \text{Fe}_{\text{final}} / \text{Fe}_{\text{initial}}$

In this test, the factorial results were analysed by the analysis of variance (ANOVA) and the significant effect was assessed by the F-test method at 95% confidence level (Montgomery, 2009). A sequential hierarchy rule in ANOVA was used to determine the best model. After performing the hierarchy rule, it was found that the Linear model is significant, as tabulated in Table 7. The main effects are significant at $\alpha = 0.05$ and a linear model could be considered in this work. All the main factors, temperature (C) and acid concentration (A) were significant. The ANOVA result also shows that the curvature is not significant, and no model transformation is required. An additional output given by Minitab 18 is the reliability value, where R^2 and R^2 adjusted for the model are 90.8% and 86.86%, respectively. R^2 adjusted has improved and is closer to R^2 implying a better statistical model is obtained.

Table 7. The analysis of variance (ANOVA) for regression modal of Fe extraction

Source	DF	Adj. SS	Adj. MS	F-Value	P-value
Model	3	6494.0	2164.68	23.03	0.001
Linear	3	6494.0	2164.68	23.03	0.001
A-Concentration	1	1804.8	1804.80	19.20	0.003
B-Time	1	1024.7	1024.69	10.90	0.013
C-Temperature	1	3664.5	3664.54	38.99	0.000
Curvature	1	193.4	193.40	2.50	0.165
Lack of Fit	4	331.3	82.82	1.24	0.491
Pure Error	2	133.2	66.59		
Cor Total	10	7151.9			

DF: Degree of Freedom; F: Fisher's test data; P: Hypothesis; Adj.SS: Adjusted Sum of Square; Adj.MS: Adjusted Mean of Square

The chosen model was verified based on the ANOVA, R^2 and R^2 adjusted. From the ANOVA results, a mathematical model in Equation 13 (coded unit) can be expressed to predict Fe extraction in the range of variables under study. It can be seen that out of the three parameters studied, temperature (C) has the most pronounced effect in enhancing Fe extraction, followed by ammonium chloride concentration(A) and leaching time (B).

$$\% \text{ Extraction of Fe} = 57.16 + 15.02A + 11.32B + 21.4C \quad (13)$$

where A - concentration of NH_4Cl , B - leaching time, C - temperature

Fig. 4 shows the main effect plot of Fe extraction. In general, Fe extraction increases as concentration (A), leaching time (B), and temperature (C) increase from low to high levels. The steepest slope of the mean response was depicted by temperature(C) in this analysis, emphasising the importance of this parameter.

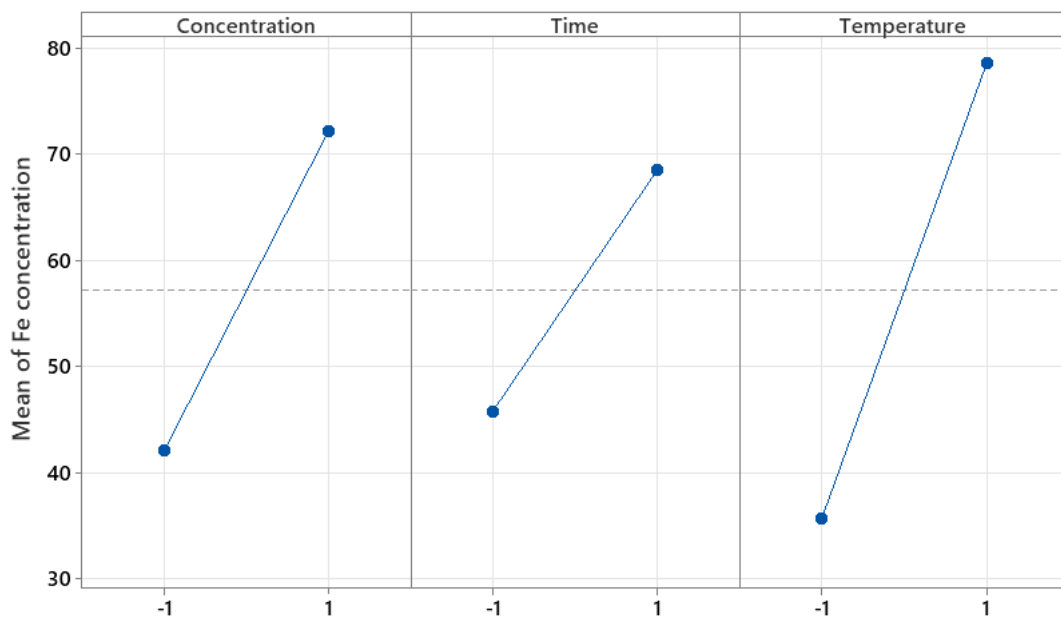


Fig. 4. Mean effect plot for each level on Fe extraction

As stated earlier, the temperature was the most significant factor affecting the aeration leaching, as shown in Run No. 2, 4, 6, and 11, which were carried out at the highest temperature. which were done at the highest temperature. This resulted in a higher value of X_{Fe} , 92.6%, 83.2%, 97.1%, and 51.7% respectively. This effect was observed as an increase in temperature will increase the leaching rate by accelerating the reaction between the ammonium ions and iron. Similar work by Sanjith, U. et al. (2019) on kinetic modelling of leaching process also observed this relationship.

Based on Fig. 5a, it can be stipulated that a higher temperature ($> 90^\circ\text{C}$) was needed to obtain a high value of X_{Fe} within a short period (< 3 hours). The effect of ammonium chloride concentration was also analysed to identify any other correlation between the concentration and temperature for aeration leaching. As shown in Fig. 5(b), a higher value of X_{Fe} could be achieved if the concentration of NH_4Cl and temperature were elevated continuously. This NH_4Cl acts as the catalyst for the leaching process that consists of NH_4^+ as a buffer for hydroxyl ion (OH^-) and averts excessively high local pH values. However, higher NH_4Cl concentration may affect the pH value, which could slow down the reaction since the iron could precipitate before the iron(II) ions leach/diffuse from the rutile matrix. The chloride ions act on breaking down the passive films, which may appear during aeration (Geetha and Surender, 2000).

This statistical design also provided the interaction between the three variables, which was in the form of a 3D-cube plot. The cube plot displays the response changes when the three factors vary (Fig. 6). From the latter Fig., the highest X_{Fe} (100%) was achieved at 90°C using 0.5M NH_4Cl in 7 hours. Meanwhile, the lowest amount of X_{Fe} (9.42%), when the temperature was at 50°C using 0.1 M NH_4Cl in 3 hours.

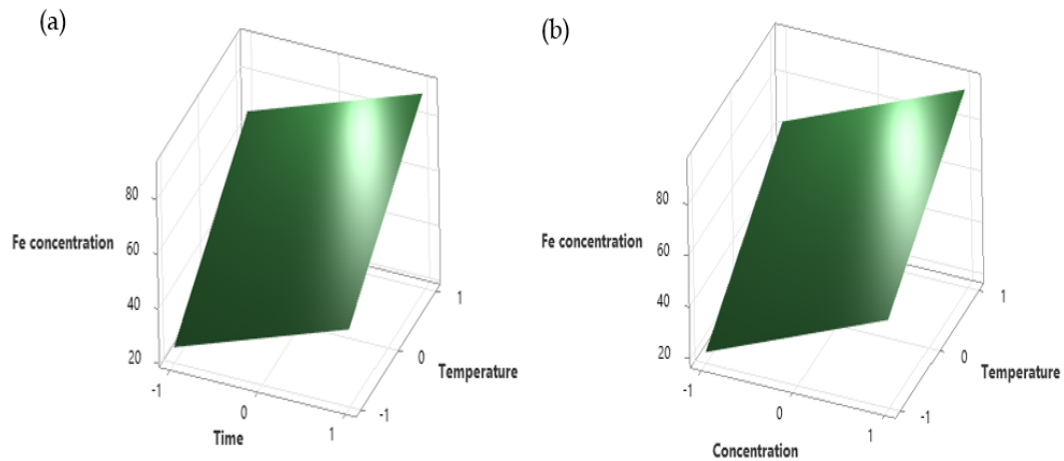


Fig. 5. The surface plot (a) Fe extraction as a function of time (B) and temperature (C); (b) Fe extraction as a function of concentration (A) and temperature (C)

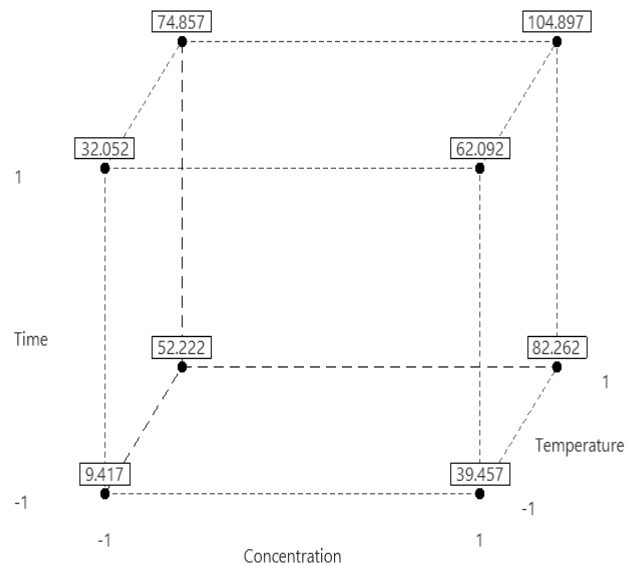


Fig. 6. 3-D Cube Plot of interaction between three variables (concentration, leaching time and temperature)

3.3. Mineralogical characterisation of leaching residue

XRD with Rietveld refinement analysis was performed on the residues to determine the mineral phases after aeration leaching. The variability of the mineral composition was taken into account by refinement and modification of crystallographic parameters of the initial minerals. XRD analysis shown in Fig. 7 compares the raw ilmenite diffraction pattern, reduced sample, and a leached sample. XRD pattern of a sample of Run No.6 (0.5 M NH_4Cl , 90 °C, 7 hours) was chosen due to the highest iron extraction ($X_{\text{Fe}}=97\%$). From the XRD patterns showed in Fig. 7, major crystalline phases such as ilmenite (FeTiO_3) in ilmenite ore were transformed into metallic iron, Ti_2O_3 (ICSD No: 01-085-0868) and Fe_3O_4 (ICSD No: 98-001-2128) in the reduced ilmenite. After the leaching process, the major mineral phases that can be identified were Ti_2O_3 , Fe_2O_3 and Ti_3O_5 (ICSD No: 98-007-1966). Rietveld analysis indicates that the leached residue contains TiO_2 (80.8%) and Fe_2O_3 (7.8%) with R_{wp} (2.43%) and GoF (1.7).

Residue from Run No.6 (90 °C, 7 hours, 0.5 M NH_4Cl concentration) was also analysed by XRF to determine the chemical composition of leached residue. From data in Table 8, major composition in the leached sample were TiO_2 (80.71%), Fe_2O_3 (8.498%), SiO_2 (2.126%), MnO (2.222%) and MgO (1.333%). In this work, low-grade Malaysia ilmenite was successfully upgraded to more than 80% TiO_2 . However, other impurities such as SiO_2 , MnO and MgO still indicated significant percentages needed to be removed in future work.

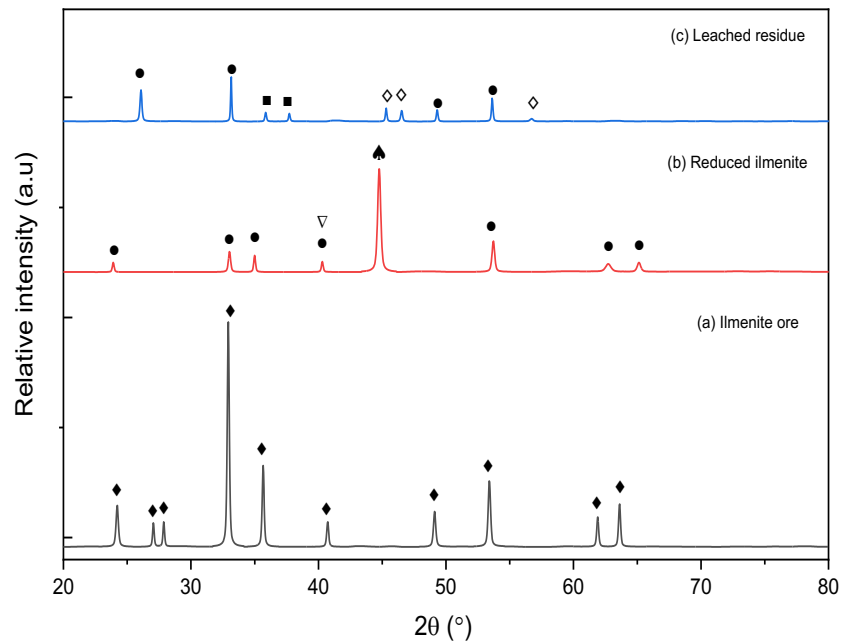


Fig. 7. XRD diffractogram patterns of the (a) ilmenite ore, (b) reduced ilmenite and (c) leached residue. (◆ FeTiO_3 ; ● Ti_2O_3 ; ▲ Fe; ▽ TiC; ■ Fe_2O_3 ; ◇ Ti_3O_5)

Table 8. Chemical composition of the sample after aeration leaching process (90 °C temperature, 7 hours for leaching time in 0.5 M NH_4Cl concentration)

Compound	Wt. (%)	Compound	Wt. %
TiO_2	80.71	CaO	0.48
Fe_2O_3	8.49	Na_2O	0.008
SiO_2	2.13	K_2O	0.013
MnO	2.22	P_2O_5	0.006
MgO	1.32		

Fig. 8 (a)-(d) represents SEM photomicrograph features of the surface morphology of the leached residue grains after 7 hours of leaching in 0.5 M NH_4Cl at 90 °C. It can be seen that the overall particle shape change as the initial dissolution takes place and is altered to a very porous surface (Fig. 8a). Another feature observed from the SEM image is the surface irregularity of the leached sample. Surface irregularity observed showed that the leaching took place in the region of metal iron and ferrous oxide sites. The EDX analysis (Fig. 8d) showed that the major element for leached residue was Ti (68 wt.%) and less than 1 wt.% Fe. Rietveld analysis supported that predominant elements in the leached residue were Ti, and almost all iron have been dissolved into solution.

4. Conclusions

The following conclusions were drawn based on the results obtained in this work:

1. Malaysian ilmenite from Bukit Kelip, Terengganu, was characterised as low-grade TiO_2 (42 wt.%).
2. Carbothermal reduction method using local carbon source (Sarawak Mukah-Balingan Coal) as reducing agent has successfully reduced iron oxide into metallic iron. The addition of compressed national gas has reduced coal usage and proved successful with complete carbothermal reduction.
3. For aeration leaching, the leaching parameters of concentration, temperature and leaching time were evaluated by the full factorial method and it was found that temperature was the most significant parameter.
4. The optimum condition for NH_4Cl concentration and temperature is 0.5 M at 90°C for 7 hours, respectively, with a high percentage extraction of iron at 97% and 81 wt.% TiO_2 in the leached residue, which is quite suitable for the production of synthetic rutile. Further improvement can be made by

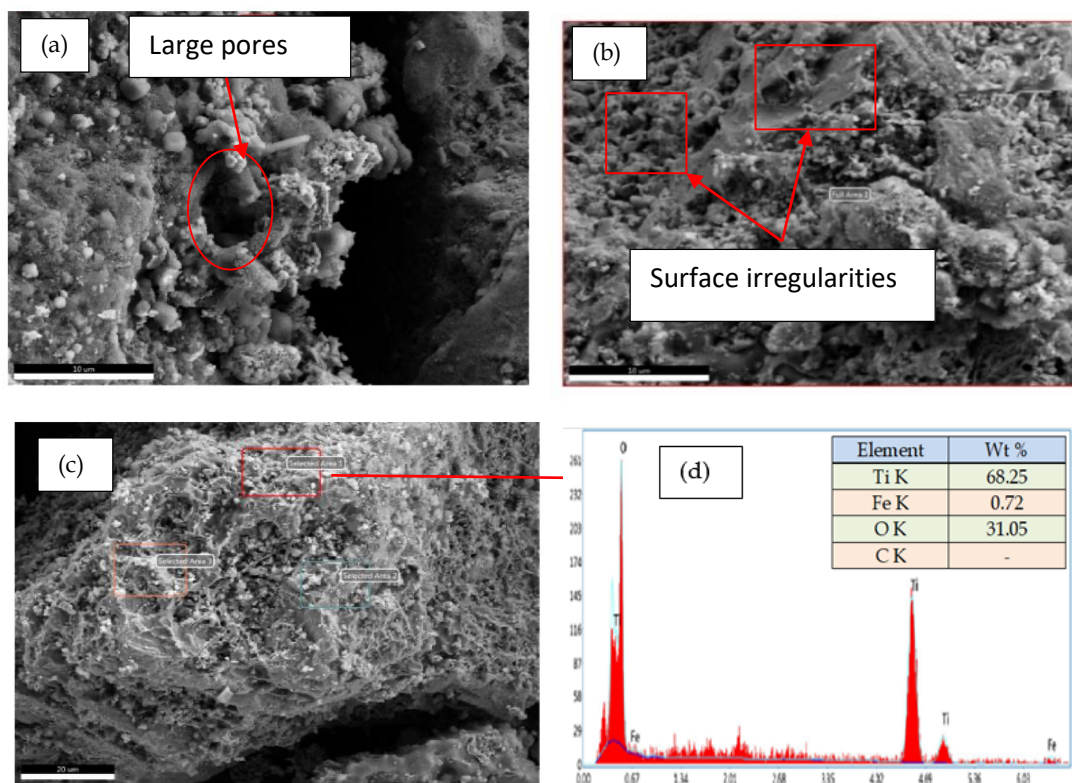


Fig. 8. SEM photomicrograph of the leached residue (90°C, 7 hours in 0.5M NH₄Cl) (a) surface morphology of the porous structure; (b) surface irregularity; (c) and (d) EDX spot analysis

removing MnO₂ through sulphur addition in the carbothermal reduction to form MnS and this could further remove more Fe.

5. The low-grade Malaysian ilmenite has the potential to be upgraded to synthetic rutile for TiO₂ industry feedstock.

Acknowledgements

The authors gratefully acknowledge the support from Universiti Sains Malaysia (USM) through USM's short term grant (304/PBAHAN/6315249) and Mineral and Geoscience Department Terengganu (JMG) for the assistance of collecting samples. Dr Sheikh Abdul Rezan also supported this research via USM Research University Individual (RUI) grant no: 1001/PBAHAN/814273. Further support was by Nippon Sheet Glass Research Grant (NSGRG) (No. 304/PBAHAN/650360/N120). Further support was also from USM technical staffs, Mr. Shahrul Ami Bin Zainal Abidin and Mr. Mohamad Shafiq Bin Mustapa Sukri for supporting the author's experimental work.

References

- ADIPURI, A., LI, Y., ZHANG, G., OSTROVSKI, O., 2011. Chlorination of reduced ilmenite concentrates and synthetic rutile. *Int.J.Min.Process.* 100, 166-171.
- AHMADI, E., FAUZI, A., HUSSIN, H., BAHARUN, N., ARIFFIN, K.S., REZAN, S.A., 2017. Synthesis of titanium oxycarbonitride by carbothermal reduction and nitridation of ilmenite with recycling of polyethylene terephthalate (PET). *Int. J. Min. Metall. and Mater.* 24, 444-454.
- AHMADI, E., SHOPARWE, N.I., IBRAHIM, N., ABDUL HAMID, S.A.R.S., FAUZI, A., ARIFFIN, K.S., HUSSIN, H., BAHARUN, N., , REZAN, S.A., 2018. The effect of experimental variables on iron removal from nitrided Malaysian ilmenite by Becher process. *Extract.*, 1383-1396.
- DEWAN, M.A., ZHANG, G., OSTROVSKI, O., 2009. Carbothermal Reduction of Titania in Different Gas Atmospheres. *Metall. Mater. Trans. B.* 40, 62-69.

- DEWAN, M.A., ZHANG, G., OSTROVSKI, O., 2010. *Phase Development in Carbothermal Reduction of Ilmenite Concentrates and Synthetic Rutile*, ISIJ International, 50(5), 647-653.
- FILIPPOU, D. AND HUDON, G. 2009. *Iron removal and recovery in the titanium dioxide feedstock and pigment industries*. JOM, 61(10), 36-42.
- FRANCIS A.A., AND EL-MIDANY, A.A., 2008. *An assessment of carbothermic reduction of ilmenite ore by statistical design*. J. Mater. Process. Techno. 199, 279-286.
- GÁZQUEZ, M. J., BOLÍVAR, J. P., GARCIA-TENORIO, R., VACA, F. 2014. *A review of the production cycle of titanium dioxide pigment*. Mater. Sci. and App. 5, 441.
- GEETHA, K. S. AND SURENDER, G. D. 2000. *Experimental and modelling studies on the aeration leaching process for metallic iron removal in the manufacture of synthetic rutile*. Hydrometallurgy, 56, 41-62.
- HAIDER, A.J., JAMEEL, Z.N., AL-HUSSAINI, I.H.M., 2019. *Review on titanium dioxide applications*. Energy Procedia. 17-29.
- HASNIYATI, M. R., ZUHAILAWATI, H., RAMAKRISHNAN, S., HAMID, S. A. R. S. A. 2014. *Mechanism and optimisation of titanium carbide-reinforced iron composite formation through carbothermal reduction of hematite and anatase*. J. Alloy. and Comp., 587, 442-450. <https://doi.org/10.1016/j.jallcom.2013.10.245>
- HEIKEN, G., RAMOS, N., DUFFIELD, W., MUSGRAVE, J., WOHLTZ, K., PRIEST, S., ALDRICH, J., FLORES, W., RITCHIE, A., GOFF, F., EPPLER, D., ESCOBAR, C. 1991. *geology of the platanares geothermal area, departamento de copán, honduras*. J. Volcano. and Geothe. Res. 45, 41-58.
- IBRAHIM, N., AHMADI, E., ABDUL RAHMAN, S., AHMAD FAUZI, M.N., REZAN, S.A., 2017. *Extraction of titanium from low iron nitrided Malaysia Ilmenite by chlorination*. AIP Conference Proceeding 1805.
- MONTGOMERY, D.C., 2009. *Design and analysis of experiments*. 7th ed. NJ: John Wiley & Sons, Inc.
- NGUYEN, T.H., LEE, M.S., 2019. *A Review on the Recovery of Titanium Dioxide from Ilmenite Ores by Direct Leaching Technologies*. Min. Pro. and Ex. Metall. Rev. 40:4, 231-247.
- REZAN, S. A., ZHANG, G. & OSTROVSKI, O. 2012a. *Effect Of Gas Atmosphere On Carbothermal Reduction And Nitridation Of Titanium Dioxide*. Metall. and Mater. Trans. B. 43, 73-81.
- REZAN, S. A., ZHANG, G. & OSTROVSKI, O. 2012b. *Phase development in carbothermal reduction and nitridation of ilmenite concentrates*. High Temp. Mater. Pro., 43, 73-81.
- SAIDIN, H. S., S. A. S. SALIM, HUSSAIN, H., REZAN, S.A.S.A.H., BAHARUN, N. 2014. *An Assessment of the Carbothermal Reduction of Malaysian Ilmenite by Statistical Design*. Adv. Mater. Res. 858, 221-227.
- SANJIT, U., CHOONG, K.W., SIVAKUMAR, R., FAUZI, M.N.A., REZAN, S.A. 2019. *Kinetic modelling of oxidation of metallic iron to iron sulfate from iron-titanium oxycarbonitride composite*. Materials Today: Proceeding 17, 525-533.
- SHARIFAH, A. S. S., SAIDIN, H. S., BAHARUN, N., REZAN, S. A., & HASHIM, H. 2013. *Microstructural Study of Reduced Malaysian Ilmenite by Carbothermal Reduction and Nitridation in Nitrogen Atmosphere*. Adv. Mater. Re. 858, 265-271.
- SHAHIEN, M.G., KHEDR, M.M.H, MAURICE, A.E., FARGHALI A.A., ALI, R.A.M., 2015. *Synthesis of high purity rutile nanoparticles from medium grade Egyptian natural ilmenite*. Beni-Seuf University Journal of Basic and Applied Science. 207-213.
- TRUONG, T.N., NGUYEN, T.T, DUONG, B.N. 2017. *Acetic acid and sodium acetate mixtures as an aeration catalyst in the removal of metallic iron in reduced ilmenite*. Acta Metall. Slovaca. 23, 371-377.
- WANG, X., LI, C., YUE, H., YUAN, S., LIU, C., TANG, S., LIANG, B., 2018. *Effects of mechanical activation on the digestion of ilmenite in dilute H₂SO₄*. Chin.J.Chem.Eng., 2019, 27, 575-586.
- WARREN J., BRUCKARD, C.C., FLETCHER, S., HORNE, M.D, URBAN A.J. 2004. *The Application Of Anthraquinone Redox Catalysts For Accelerating The Aeration Step In The Becher Process*. Hydrometallurgy, 73, 111-121.
- XIANG, J., PEI, G., LV, W., LIU, S., LV, X., QIU, Q. 2020. *Preparation of synthetic rutile from reduced ilmenite through the aeration leaching process*. Chem. Eng. & Pro.: Pro. Intensific. 147, 1-9.
- YAAKUB, K.N.H. AND A.H.A. RAHMAN, *Kajian Potensi Sumber Ilmenite Di Sungai Cheniah Bukit Kelip, Hulu Dungun, Terengganu, in Rancangan Malaysia ke sepuluh. Projek mineral berlogam semenanjung*. 2014: Kuala Terengganu. p. 10
- YARAGHIA, A., SAPRI, A., AHMADI, E., BAHARUN, N., REZAN, S.A., SHOPARWE, N.I., RAMAKRISHNAN, S., ARIFFIN, K.S., AHMAD FAUZI, M.N., ZABIDI, H., ISMAIL, H., HAZMAN H.S., 2011. *Microstructural Study of Leached Nitrided Malaysian Ilmenite with Coal-Polystyrene Reductant*. Key Engineering Materials: 701, 132-137.

- YIN, T.W., RAMAKRISHNAN, S., ABDUL REZAN, S., MOHD NOOR, A.F., SHOPARWE N.I., ALIZADEH, R., ROOHI, R. 2017. *Kinetic modeling of liquefied petroleum gas (LPG) reduction of titania in MATLAB*. J. of Phy.: Conf. Series, 822, doi:10.1088/1742-6596/822/1/012063.
- ZHANG, W., ZHU, Z., CHENG, C.Y. 2011. *A Literature Review Of Titanium Metallurgical Processes*. Hydrometallurgy, 108, 177-188.